Journal of Solid State Chemistry 181 (2008) 1859–1866

Contents lists available at ScienceDirect

Journal of Solid State Chemistry

journal homepage: www.elsevier.com/locate/jssc

Oxidation/reduction studies on $Zr_yU_{1-y}O_{2+x}$ and delineation of a new orthorhombic phase in U–Zr–O system

S.K. Sali [a,*], N.K. Kulkarni [a], K. Krishnan [a], S.N. Achary [b], A.K. Tyagi [b]

[a] Fuel Chemistry Division, Bhabha Atomic Research Centre, Trombay, Mumbai 400 085, India
[b] Chemistry Division, Bhabha Atomic Research Centre, Trombay, Mumbai 400 085, India

ARTICLE INFO

Article history:
Received 13 November 2007
Received in revised form
22 March 2008
Accepted 30 March 2008
Available online 11 April 2008

Keywords:
X-ray diffraction
Crystal structure
Thermogravimetry
Uranates

ABSTRACT

In this communication, we report the oxidation and reduction behavior of fluorite type solid solutions in U–Zr–O. The maximum solubility of ZrO_2 in UO_2 lattice could be achieved with a mild oxidizing followed by reducing conditions. The role of valency state of U is more dominating in controlling the unit cell parameters than the incorporated interstitial oxygen in the fluorite lattice. The controlled oxidation studies on U–Zr–O solid solutions led to the delineation of a new distorted fluorite lattice at the U:Zr = 2:1 composition. The detailed crystal structure analysis of this ordered composition $Zr_{0.33}U_{0.67}O_{2.33}$ (ZrU_2O_7) has been carried from the powder XRD data. This phase crystallizes in an orthorhombically distorted fluorite type lattice with unit cell parameters: $a = 5.1678(2)$, $b = 5.4848(2)$, $c = 5.5557(2)$ Å and $V = 157.47(1)$ Å^3 (Space group: *Cmcm*, No. 63). The metal ions have distorted cubical polyhedra with anion similar to the fluorite structure. The excess anions are occupied in the interstitial (empty cubes) of the fluorite unit cell. The crystal structure and chemical analyses suggest approximately equal fractions of U^{4+} and U^{6+} in this compound. The details of the thermal stability as well as kinetics of formation and oxidation of ZrU_2O_7 are also studied using thermogravimetry.

1. Introduction

Thermophysical properties of zirconia-based inert materials are of recent interest since zirconia containing pyrochlore ($A_2B_2O_7$) or fluorite (MO_2) structures have been proposed as suitable materials for fixation of actinides from high level nuclear waste (HLW) [1]. The room temperature monoclinic phase of Zirconia (ZrO_2) transforms to tetragonal phase at 1443 K and to cubic (fluorite type) phase at 2643 K. The high temperature phase of ZrO_2 can be stabilized by tetravalent (Ce^{4+}, Th^{4+} and U^{4+}) [2], trivalent (Rare earths) [3] and divalent (Ca^{2+}, Mg^{2+}) cations. It is well reported that the actinide (*An*) oxides can stabilize the high temperature cubic (fluorite) lattice of ZrO_2 forming a solid solution. However, actinide oxides can form solid solutions in a very limited range with monoclinic and tetragonal lattices of ZrO_2 [4,5]. The solid solubility of ZrO_2 in actinide oxide increases with decrease in size of actinide ion. Thus solubility of ZrO_2 in ThO_2, UO_2 and PuO_2 is 5, 20 and 80 mol% at 1673 K, respectively. The solubility of ZrO_2 in UO_2 forming fluorite type phase is very limited due to large differences in ionic radii of metal ions (ionic radii: Zr^{4+} 0.84 Å and U^{4+} 1.00 Å). However, the solubility increases from 13 to 35 mol% with increase in temperature from 1473 to 2148 K, respectively. In addition to the fluorite and related solid solutions, trivalent actinides do form pyrochlore phases with zirconia depending on the radii of the A and B cations (radius ratio, R_A:R_B ranges between 1.46 and 1.80). Several zirconia-based actinide pyrochlores, viz. $An_2Zr_2O_7$ (*An* = Pu, Am, Cm, Bk, Cf etc.) have been reported in literature [1,6,7].

The knowledge of phases and thermodynamic properties of the MO_2–ZrO_2 (M = actinide element) is necessary to interpret and predict the properties of these materials. The crystal chemistry, thermodynamic and magnetic properties of fluorite-type of solid solution $M_yU_{1-y}O_{2+x}$ ($M = M^{2+}$, M^{3+} and M^{4+}) in uranium dioxide host lattice have been reviewed by Fujino and Miyake [8]. The phase diagrams in U–Zr–O system, established by various research groups show remarkable differences. Most of the phase diagrams and thermodynamic data available for ZrO_2–UO_2 system have been critically evaluated by Yashima et al. [9]. Earlier, oxygen potential for $Zr_{0.15}U_{0.85}O_{2+x}$ solid solution has been measured thermogravimetrically by Une and Oguma [10]. Solid solubility of ZrO_2 in UO_2 at different annealing temperatures from 1473 to 2373 K was reported by Cohen and Schaner from X-ray diffraction and metallographic studies [11]. Also the variation of the lattice parameter with zirconium concentration of the cubic solid solution $Zr_yU_{1-y}O_{2.00}$ has been reported [12]. An apparently continuous sequence of ordered orthorhombic fluorite related super structures near $U_2Zr_5O_{15}$ compositions (U, Zr)O_{2+x}, $0.114 < x < 0.154$) have been reported [13].

* Corresponding author. Fax: +91 22 5505151.
E-mail address: sksali2002@yahoo.com (S.K. Sali).

0022-4596/$ - see front matter © 2008 Elsevier Inc. All rights reserved.
doi:10.1016/j.jssc.2008.03.039

The present study describes preparation and characterization of the ZrO_2–UO_2 solid solution in controlled oxidative and reductive environments. In addition, the oxidation behavior of the U–Zr–O solid solutions with U^{4+} ions led to the delineation of a new phase in U–Zr–O system at composition $Zr_{0.33}U_{0.67}O_{2.33}$. The main focus of this study is the formation, crystal structure, thermal stability and kinetics of oxidation of this new $Zr_{0.33}U_{0.67}O_{2.33}$ phase.

2. Experimental

2.1. Synthesis

ZrO_2 (BDH 99.9%) and $UO_{2.00}$ were used as starting materials. Uranium oxide with O/U of 2.00 was obtained by reduction of nuclear grade UO_{2+x} in argon gas with 8% (v/v) hydrogen at 1073 K for 3 h. Homogenous mixtures of UO_2 and ZrO_2 with different molar ratio (90:10, 80:20, 70:30, 65:35 and 60:40) were prepared by grinding together in an agate mortar. The corresponding compositions were also prepared by gel combustion method using standard solutions of uranyl nitrate and zirconium nitrate [14]. The homogenous mixtures obtained in both methods were heated at 1673 K for 48 h in a commercial argon atmosphere. The product obtained after this heat treatment were reground and pressed into pellets and further heated at 1673 K for about 10 h in 8% (v/v) H_2:Ar atmosphere. The products after each heat treatment were analyzed by X-ray powder diffraction (XRD) analysis using monochromatized Cu-$K\alpha_1$ radiation ($\lambda = 1.5406$ Å) on a STOE X-ray diffractometer. The comparison of the powder XRD patterns indicates the existence of a new phase of composition $Zr_{0.35}U_{0.65}O_{2+x}$. Further studies were carried out with oxidized product of the $Zr_{0.33}U_{0.67}O_{2+x}$ prepared under the same conditions.

2.2. Characterization of new $Zr_{0.33}U_{0.67}O_{2+x}$ phase

The uranium content in the new phase was estimated by chemical analyses for U(IV) and total uranium. For the analysis of total uranium, Fe(II) was used for reduction of U(VI) to U(IV) in concentrated (10 M) phosphoric acid medium [15]. Un-reacted excess Fe(II) was oxidized with dilute nitric acid in presence of molybdenum (VI) as catalyst and U(IV) was determined by direct potentiometric titration with $K_2Cr_2O_7$ solution. The entire titration was carried out on weight basis.

Uranium to zirconium ratio was determined by Energy Dispersive X-ray Fluorescence (EDXRF) analysis (JORDAN VALLEY model EX-3600 TEC with Rh as target material). Synthetic standards prepared by mixing known amounts $UO_{2.667}$ and ZrO_2 in different molar proportions to cover the range of U/Zr ratio from 1:2 to 4:1, were used for calibration. For quantitative analysis intensity ratio of U $L\alpha$ and Zr $K\alpha$ against U to Zr atom ratio was used.

The oxygen analysis was done by thermogravimetry (TG) using Mettler Thermoanalyzer (model: TGA/SDTA851^e/MT5/LF1600). The thermoanalyzer was calibrated from the decomposition of 100 mg of $CaC_2O_4 . H_2O$ to CaO during heating to 1273 K. Non-isothermal kinetic studies of the formation of new phase ($Zr_{0.33}U_{0.67}O_{2+x}$) up to 873 K in air and its oxidation up to 1473 K was studied by heating the samples at 10 K/min in thermoanalyser. The thermal stability of the new compound was studied in different atmospheres such as Ar/8%H_2, He, CO_2 and air.

The density of the new compound was determined by using pycknometric method using toluene as medium and also by gas displacement method.

The powder diffraction data for crystal structure refinement for the new phase was collected in the two theta range of 8–100° with step of 0.02° and a counting time of 5 s for each step. The diffraction data were analyzed using the program EXPO2004, Fullprof 2K and GSAS software packages [16–18].

3. Results and discussion

3.1. Synthesis and characterization

The powder XRD patterns of the samples prepared by the preliminary heat treatment in argon atmosphere as well as subsequent reduction in Ar/8%H_2 atmosphere show the typical fluorite type phase up to $y = 0.35$. The unit cell parameters of the fluorite type phases obtained from solid state as well as gel combustion method were found to be similar. The observed unit cell parameters of $Zr_yU_{1-y}O_{2.00}$ ($y = 0.1$, 0.2, 0.3 and 0.35) are summarized in Table 1. The unit cell parameters of the samples prepared by this modified reductive procedure agree well with the reported lattice parameters for $(U,Zr)O_{2.00}$ solid solutions prepared by direct heating at 2023 K in H_2 atmosphere [11]. A comparison of the unit cell parameters of the fluorite type phase obtained after the first and second heat treatment shows higher value for the later ones. However, in both cases the unit cell parameters shows a decreasing trend, with increasing ZrO_2 content. The formation of solid solution of ZrO_2 in UO_2 lattice is well known in Ar/8%H_2 atmosphere, but the solubility limits to only 15 mol% at 1673 K [11]. The limited solubility of ZrO_2 in UO_2 can be assigned to the considerable mismatch in ionic sizes between Zr^{4+} and U^{4+}. Normally, the solid solutions are prepared by directly heating UO_2 and ZrO_2 in Ar/8%H_2 atmosphere at 1673 K for 4–10 h. In general, size of metal ion, oxidation state and structure are the important parameters for controlling the solubility of metal oxide in UO_2. However, in the present studies, the preparative conditions have been modified to attain maximum solubility. The oxide mixtures were initially heated in commercial argon gas, having 10–20 ppm oxygen impurity, up to 1673 K for 48 h, before heating in Ar/8%H_2 up to 1673 K for 10 h. In the second step, the $(U,Zr)O_{2+x}$ is reduced to stoichiometric $(U,Zr)O_{2.00}$ composition.

A comparison of the unit cell parameters of the solid solutions prepared after heating in commercial argon and those prepared after heating Ar/8%H_2 mixture suggests two types of non-stoichiometric phases, namely, $Zr_yU_{1-y}O_{2+x}$ and $Zr_yU_{1-y}O_{2.00}$. The lattice parameters for $Zr_yU_{1-y}O_{2.00}$ compositions are higher owing to the larger ionic radius of U^{4+} formed by the reduction of U^{5+} or U^{6+} in $Zr_yU_{1-y}O_{2+x}$. This was further supported by chemical analysis of U(IV) and total uranium in solid solution at every stage of preparation. With further increase in zirconium concentration up to 40 mol%, fluorite type phase along with tetragonal ZrO_2 was observed in XRD pattern indicating 35 mol% as the limit of

Table 1
Lattice parameter of $Zr_yU_{1-y}O_2$ ($y = 0.1$, 0.2, 0.3, 0.35 and 0.4 solid solution after heating in commercial argon and in Ar/8%H_2 atmosphere

Composition	Lattice parameter of fcc phase (Å) after heating in	
	Commercial Ar at 1673 K	Ar/8%H_2 at 1673 K
0.9 UO_2+0.1 ZrO_2	5.385	5.440
0.8 UO_2+0.2 ZrO_2	5.356	5.410
0.7 UO_2+0.3 ZrO_2	5.327	5.380
0.65 UO_2+0.35 ZrO_2	5.315	5.365
0.6 UO_2+0.4 ZrO_2	5.305[a]	5.365[a]

[a] Indicates phase contaminated with tetragonal ZrO_2.

solubility of ZrO_2 in UO_2 at 1673 K. The initial heating of UO_2 and ZrO_2 mixture in commercial argon helps in oxidizing UO_2 to UO_{2+x}, thereby decreasing the UO_2 unit cell parameters due to oxidation of U^{4+} to U^{5+}/U^{6+}. As the mismatch in ionic size between Zr^{4+} and U^{5+}/U^{6+} is reduced, the solubility of ZrO_2 in UO_2 increases. The opposite role of interstitial oxygen atoms in controlling the unit cell parameters is overcompensated with the drastic decrease in the ionic radii mismatch of the metal ion site with increase in oxidation state of uranium. In addition, this modified two steps heating process helps in increasing the solubility of ZrO_2 in UO_2 up to 35 mol% at 1673 K [19].

Thermogravimetry (TG) studies on $Zr_yU_{1-y}O_{2.00}$ for ($y = 0.1$–0.35) was carried out in air up to 1473 K. For $y = 0.1$ and 0.2, the oxidation occurred in a single step and the XRD pattern of the oxidized product at 1173 K was found to be α-U_3O_8 except some shift in the line positions. This indicates solubility of ZrO_2 in α-U_3O_8 phase. The solubility of ZrO_2 in α-U_3O_8 has been earlier reported by Pepin and McCarthy [20]. In case of $y = 0.3$, the oxidized product at 873 K was found to be a mixture of a new phase and U_3O_8. However, the oxidation of the solid solutions with $y = 0.35$ occurred in two steps. The first step is up to 873 K and the XRD pattern of the oxidized product is different from any of the reported phase in U–Zr–O system. Further oxidation in air above 1173 K gave a mixture of α-U_3O_8 containing ZrO_2 and additional tetragonal phase of ZrO_2. This oxidation behavior is similar to the oxidation of UO_2, which oxidizes in air to the tetragonal U_3O_7 phase up to 623 K and orthorhombic U_3O_8 phase at 1073 K [21]. So the further studies were mainly focused on solid solution of composition $Zr_{0.33}U_{0.67}O_{2.00}$ expecting a U_3O_7 related phase.

Fig. 1 shows the typical TG, DTA and DTG curves for the oxidation of the solid solution of composition $Zr_{0.33}U_{0.67}O_{2.00}$ up to 1473 K in air. The analysis of the TG curves indicates the total mass gain occur in two steps, viz. 2.21% in the temperature range 473–873 K and 1.0% in the temperature range 1173–1373 K. Each step was accompanied by exothermic DTA peaks. The DTG curve showed single peak in each step indicating a single reaction. XRD pattern of the 1373 K heated product revealed the presence of a solid solution of ZrO_2 with α-U_3O_8. Total observed mass gain of 3.2% corresponds to mass gain of 0.44 oxygen atoms (expected mass gain is 3.19%). XRD pattern of 873 K heated product was different from any of the reported phase in U–Zr–O system. To characterize the 873 K heated product, chemical analysis of total uranium and U(IV) was carried out. Table 2 shows the results of chemical, TG and EDXRF analysis of the new phase. As seen from this table, $U(IV)/U_{total}$ is around 50%, indicating the average valency of uranium in new compound to be U(V). The corresponding O/(U+Zr) in the new phase was found to be 2.32. The oxidation of $Zr_{0.33}U_{0.67}O_{2.00}$ up to 873 K showed weight gain of 2.21%, corresponding to 0.31 oxygen gain and this indicates that the O/(U+Zr) in the new phase is 2.31. Fig. 2 shows the calibration plot of the intensity ratios of U/Zr vs uranium to zirconium atom ratios by EDXRF method. U/Zr atomic ratio in the new phase was found to be 1.84. Thus the results of chemical, TG and EDXRF analysis showed that the composition of new phase is $Zr_{0.33}U_{0.67}O_{2.33}$ which is equivalent to ZrU_2O_7 and this phase is similar to composition U_3O_7 in U–O system. This partial oxidized product was further characterized in detail by X-ray diffraction.

3.2. Crystal structure of $(Zr_{0.33}U_{0.67})O_{2.33}$

The observed diffraction data was indexed using the *Treor* subroutine of the *Fullprof-2K* software package [17]. An orthorhombic lattice with unit cell parameters, $a = 5.556(2)$, $b = 5.490(2)$ and $c = 5.169(1)$ Å was obtained as the best solution for the present diffraction data. Further the unit cell parameters

Table 2
Characterization of the new phase by chemical, thermogravimetry (TG) and energy dispersive X-ray fluorescence (EDXRF) analyses

Analysis	Observed	Calculated
Chemical		
Total U (Wt %)	70.03	70.12
U(+4) (Wt%)	37.11	35.06
Thermogravimetry		
% Wt. gain for $Zr_{0.33}U_{0.67}O_{2.00} \rightarrow$ new phase	2.21	2.41
EDXRF		
U/Zr atomic ratio	1.84	2.00

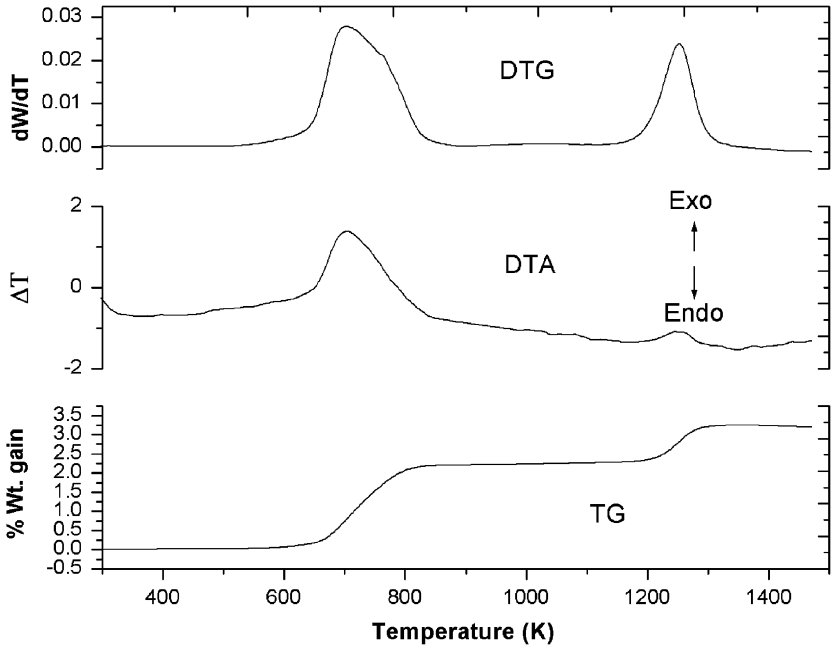

Fig. 1. TG, DTA and DTG of $Zr_{0.33}U_{0.67}O_{2.00}$ in air.

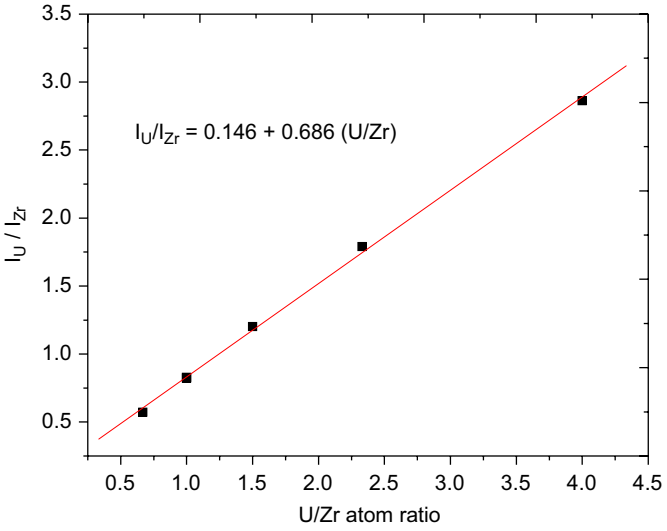

Fig. 2. Calibration plot of intensity ratio vs. U/Zr atomic ratio of synthetic standards.

were refined with *Celref* subroutine available in *Crysfire suite* [22]. The best space group *Cmcm* (No. 63) and *Ama2* (No. 40) were selected from the typical systematic extinction. The typical observed and calculated reflections for ZrU_2O_7 along with their indices are given in Table 3. The observed unit cell parameters closely resemble to the normal fluorite type UO_2 and related UO_{2+x} phases (namely, U_4O_9, U_3O_7, U_2O_5, U_3O_8 etc. [23–25]), but with a small orthorhombic distortion. In addition, the major reflections are very similar to the reported tetragonal U_3O_7 (JCPDS-PDF 15-0004). However, no suitable structure model could be obtained for these cell parameters from these reported phases. The values of these observed unit cell parameters suggest a possible distortion in the fluorite lattice either due to cation ordering or due to excess anions in the lattice. The preparation method and observed density support excess anions in the unit cell. The anion excess UO_{2+x} structures are known to form a series of ordered structures with integral or non-integral O/U ratio [24]. The anion excess fluorite structured oxides or fluorides are well known for their rich crystal chemistry with distortion originating from ordering of cations as well as anions [25,26]. In addition, the ordered phases in these systems do have a phase width arising from the cation intermixing allowing a narrow width of oxygen or fluorine.

The space group *Cmcm* (No. 63) was used to elucidate the crystal structure of this compound. This space group being centro-symmetric is more preferred than the non-centro-symmetric Ama2 space group. For generating the structural model the integrated intensities were extracted and solved using EXPO2004 software package [16]. The final Fourier calculations suggest three peaks, corresponding to two-distinct oxygen and a metal ion. Based on these generated atom positions the Rietveld refinement of the observed powder XRD data were carried out using the GSAS software package [18]. The background was modeled with shifted Chebyschev function with 18 terms. The Pseudo-Voigt profile function was used to generate the diffraction profile. Asymmetry and particle size broadening term were corrected in the profile function. Initial cycles of refinements were made with the background and scale along with the unit cell parameters, and then profile parameters and preferred orientation were included. No significant contribution from the preferred orientation is observed in the refinements. The residuals of the refinements as well as the refined position coordinates along with their thermal

Table 3
Indexed X-ray powder diffraction data of $Zr_{0.33}U_{0.67}O_{2.33}$ (ZrU_2O_7)

d_{obs}	d_{cal}	I/I_0	1			2		
			h	*k*	*l*	*h*	*k*	*l*
3.7628	3.7613	9	0	1	1	1	1	0
3.1160	3.1146	100	1	1	1	1	1	1
2.7785	2.7778	16	2	0	0	0	0	2
2.7378	2.7424	11	0	2	0	0	2	0
2.5850	2.5839	5	0	0	2	2	0	0
2.4592	2.4591	5	1	2	0	0	2	1
2.2353	2.2345	3	2	1	1	1	1	2
1.9517	1.9516	10	2	2	0	0	2	2
1.8845	1.8806	15	0	2	2	2	2	0
1.7816	1.7813	6	1	2	2	2	2	1
1.7231	1.7236	6	0	3	1	1	3	0
1.6612	1.6614	10	3	1	1	1	1	3
1.6443	1.6461	7	1	3	1	1	3	1
	1.6434		0	1	3			
1.5762	1.5759	10	1	1	3	3	1	1
1.5586	1.5573	7	2	2	2	2	2	2
1.4646	1.4646	3	2	3	1	1	3	2
1.3906	1.3889	2	4	0	0	0	0	4
1.3308	1.3313	2	1	4	0	0	4	1
1.2941	1.2941	2	0	0	4	4	0	0
1.2582	1.2584	2	1	0	4	0	1	2
1.2259	1.2292	4	3	1	3	3	1	3
	1.2230		1	3	3			
1.1831	1.1834	3	1	4	2	2	4	1
1.1714	1.1714	3	2	0	4	4	0	2
1.1430	1.1427	3	2	3	3	3	3	2
1.0780	1.0778	3	2	2	4	4	2	2
1.0381	1.0382	1	3	3	3	3	3	3

1. Space group: *Ama2* ($a = 5.5556$, $b = 5.4848$, $c = 5.1678$ Å).
2. Space group: *Cmcm* ($a = 5.1678$, $b = 5.4848$, $c = 5.5556$ Å).
($\lambda = 1.5406$ Å).

Table 4
X-ray diffraction data collection and refinement parameters

Formula	$Zr_{0.33}U_{0.67}O_{2.33}$
Crystal system	Orthorhombic
Space group	*Cmcm* (NO. 63)
Unit cell parameters (*a*, *b*, *c* in Å and *V* in Å^3)	5.1678(2)
	5.4849(2)
	5.5557(2)
	157.47(1)
Z	4
Density (X-ray)	9.56 g/cc
Measured	9.58 g/cc
Background	Chebyschev polynomial
Profile	Pseudo-Voigt
Residuals of refinement	*Rwp* = 10.8%
	Rp = 7.98%
	R_B = 6.50%

parameters are given in Tables 4 and 5, respectively. The typical Rietveld refinement plot for ZrU_2O_7 is shown in Fig. 3.

The analysis of the refined position coordinates shows that O1 atoms form a cubical surrounding around the metal atoms with typical *M*–O distances 2.28(1) to 2.42(1) Å similar to the parent fluorite lattice. The extra oxygen atoms (O2) are occupied in the empty cubes of the analogous fluorite lattice. In each of the empty cubes two sites are occupied by O2 atoms. The Rietveld refinement also confirms the random distribution of the Zr and U atoms in the lattice. The typical inter-atomic distances derived from the refined structural parameters are given in Table 6. The distorted $M(O1)_8$ cubes are connected by sharing all the edges

forming three-dimensional lattices. The empty cubes of the normal fluorite type arrangements are partially occupied (about 44%) by O2 atoms. The distance between two O2 atom sites inside a cube is extremely short, which attributes to a statistical occupancy with geometrical constraint. A typical three-dimensional arrangements of the cubes with the interstitial oxygen atoms are shown in Fig. 4. The *M* ion is bonded to four O2 atoms at a distances of 1.93(2) Å × 2 and 2.10(2) Å × 2. At a relatively longer distance, viz. 2.92(1) Å four additional O2 atoms are bonded to the metal ions. A typical surrounding of the *M* site including the distorted cubic unit is shown in Fig. 5. A reasonably short bond length of 1.93 Å might be arising from the higher oxidation state U. Besides, significantly short O1–O2 and O2–O2 are observed in this structure. Such short anion-anion contact can be explained due to disordered partially occupied anion positions, which do not have any geometrical significance. The inter-anion repulsion is maintained in the lattice by the statistical occupancy of anions with reasonable inter-atomic separation. The bond valence sums (BVSs) [27] for various bonds surrounding the *M* atoms are given in Table 6. The BVS for the cations considering a limiting distances of 2.5 Å are found to be 4.60. These observed values are significantly lower than the expected values for metal ion. Hence, the charge balance is expected to arise from longer distance anions.

A comparison of the observed structural model and composition shows a close similarity between this new compound and stoichiometric U_3O_7. A comparison of the XRD pattern also supports a close resemblance to U_3O_7. The crystal chemistry of U_3O_7 have been extensively studied and reported as the cubo-octahedron clusters of the anions as the building block of the structure [22–25]. It needs to be mentioned here, the α, β and γ phases of U_3O_7 crystallize in tetragonal lattice with c/a close to 1, whereas δ-U_3O_7 crystallizes in a monoclinic distortion in the tetragonal lattice [23]. The difference between the tetragonal and monoclinic U_3O_7 is still debatable. However, all the phases are closely interrelated and also related to the parent fluorite lattice [24–26]. A close look for the crystal chemistry of U–O system indicates a change over of fluorite to layered type lattice with $O/M \sim 2.50$. The analysis of the present observed crystal structure of ZrU_2O_7 suggests a fluorite derived structure instead of layered structure. The detailed structural studies on anion excess UO_2 compounds show the presence of long range ordering in the lattice, leading to multiple fluorite unit cell. However, in the present diffraction pattern, we could not observe any super structure reflections attributable to multiple fluorite unit cell. But, the presence of long range ordering cannot be excluded in the present case too.

A comparison of the normal fluorite structure to the present structure it can be assumed the excess anions are occupied in the interstitials, which further repel the normal lattice site anions. According the present model about 23% anions of the normal fluorite sites are unoccupied with extra 40% in the interstitials sites. However, no anion or metal site ordering or cluster ordering

Table 5
Refined position co-ordinates, occupancies and isotropic displacement parameters $(Å)^2$ for various atoms in $Zr_{0.33}U_{0.67}O_{2.33}$

	Wyc.	*x*	*y*	*z*	Occ.	Uiso
U	4*c*	0	0.2081(1)	0.25	0.66667	0.0231(3)
Zr					0.33333	0.0231(3)
O1	8*e*	0.271(2)	0	0	0.76(1)	0.076(4)
O2	8*g*	0.657(3)	0.356(4)	0.25	0.41(1)	0.061(8)

Table 6
Typical inter-atomic distances (Å) in $Zr_{0.33}U_{0.67}O_{2.33}$

	O1 *occ. 0.72(2)*	O2 *occ. 0.44(2)*	
Zr/U	2.284(7) × 2	1.93(2) × 2	
(*0.333*:*0.667*)	*0.387*/*0.625*	*0.95*/*1.53*	
	2.424(6) × 2	2.10(2) × 2	
	0.259/*0.418*	*0.635*/*1.026*	
		2.923(6) × 4	
		0.069/*0.112*	
		3.52(2) × 2	
O1–O1	2.35(3)	O1–O2	1.69(1)
O1–O1	2.75(1)	O1–O2	2.43(2)
O1–O1	2.78(1)	O1–O2	2.75(2)
O1–O1	2.818(3)	O1–O2	3.13(2)
		O1–O2	3.33(2)
O2–O2	1.67(4)	3.15(2)	3.49(4)
O2–O2	2.89(1)	3.19(2)	3.52(2)

Italic numbers are bond valences for each type bond.
Bond valences are calculated by Brown–Altermatt formula [27].
$d_0 = 1.928$ Å (for Zr–O) and 2.105 Å (for U–O); $B = 0.37$.

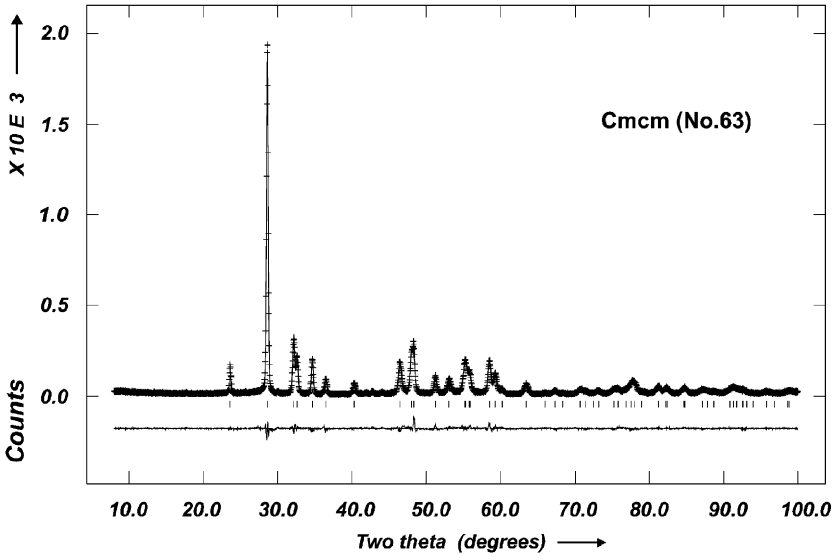

Fig. 3. Typical Rietveld refinement plot for $Zr_{0.33}U_{0.67}O_{2.33}$.

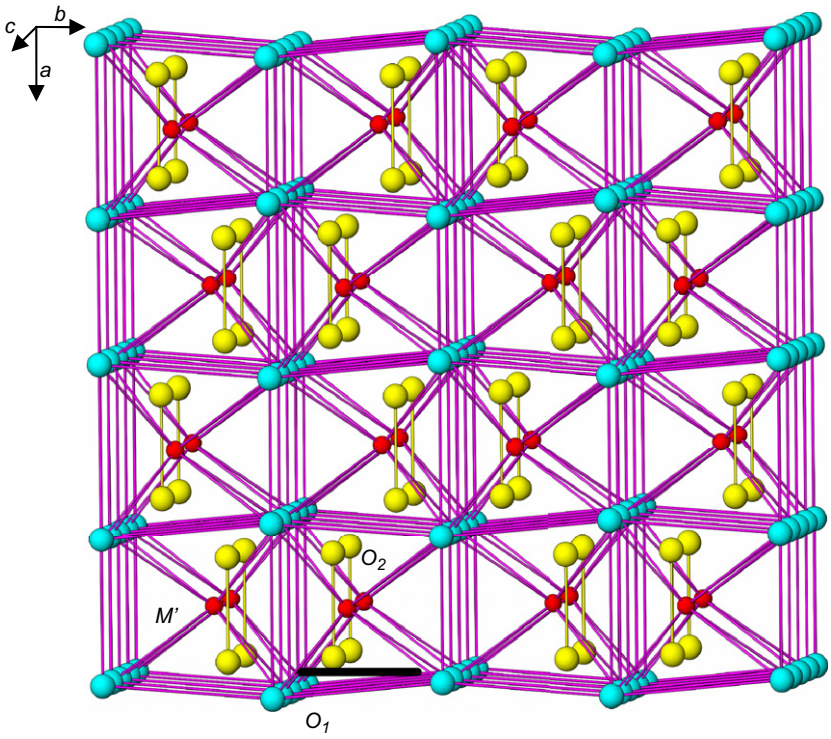

Fig. 4. Typical three-dimensional structural representation of $Zr_{0.33}U_{0.67}O_{2.33}$.

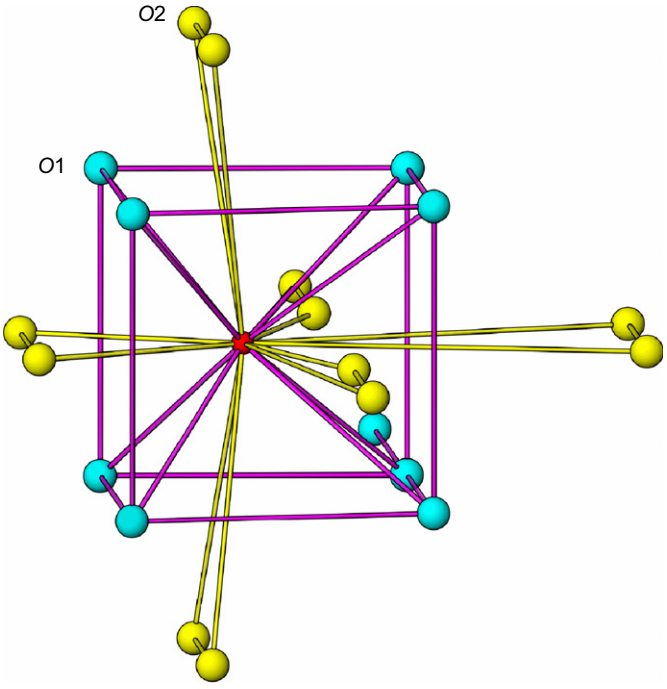

Fig. 5. Typical surroundings of oxygen atoms around the *M* atoms.

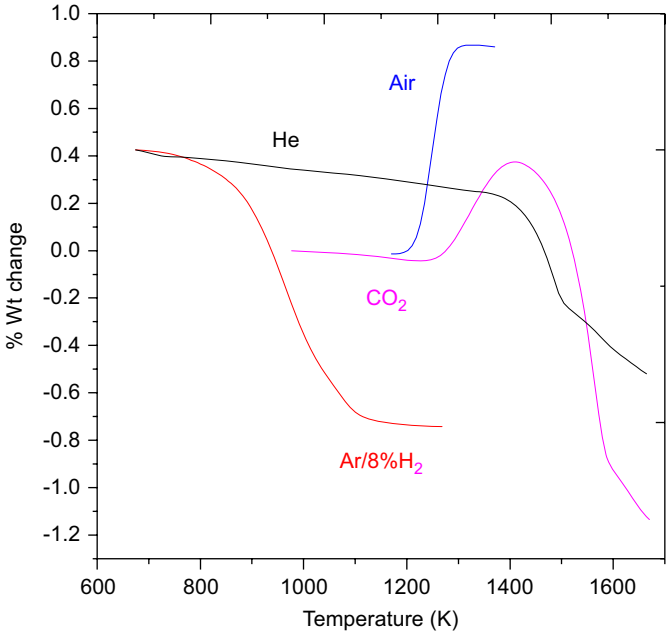

Fig. 6. Thermal stability of ZrU_2O_7 in different atmospheres.

could be revealed in this study. The absence of any super structure lines in X-ray diffraction might be the limitation arising from the drastic differences in the scattering powers of the cations and anions. Electron diffraction coupled with neutron diffraction studies are essential to reveal the exact defect model of this structure, which are being planned and will be communicated later.

3.3. Thermal studies

In order to examine the thermal stability of ZrU_2O_7 in different atmospheres, thermograms of ZrU_2O_7 were recorded in air, CO_2, He and Ar/8%H_2 atmospheres. Fig. 6 shows TG of ZrU_2O_7 in air, CO_2, He and Ar/8%H_2 atmosphere. Table 7 gives temperature range of instability, % weight gain/loss and end product formed when

ZrU_2O_7 was heated in different atmospheres. As seen from the Fig. 6, ZrU_2O_7 was found to be stable in air up to 1173 K and was oxidized in the temperature range 1173–1373 K to ZrO_2+α-U_3O_8. However, in the temperature range of 1373–1673 K, a mass loss of 1.24% was observed when heated in helium atmosphere. The XRD pattern of the end product indicates fluorite type phase with lattice parameter 5.313 Å. Thus, it can be concluded that ZrU_2O_7 is unstable in inert atmosphere above 1373 K and loses oxygen forming a fluorite type $Zr_{0.33}U_{0.67}O_{2+x}$ solid solution. However, when ZrU_2O_7 was heated in CO_2 atmosphere, a weight gain in the temperature range 1213–1373 K indicated oxidation but before the completion of oxidation, decomposition was observed. A similar decomposition behavior was also observed in helium atmosphere except for the oxidizing step. On heating in Ar/8%H_2 atmosphere, ZrU_2O_7 lose weight above 873 K and finally converts to fluorite type phase with lattice parameter 5.350 Å at 1273 K. In summary, ZrU_2O_7 on heating in CO_2, He and Ar/8%H_2 atmosphere converts to fluorite type phase $Zr_{0.33}U_{0.67}O_{2+x}$ with varying lattice parameters as seen from Table 7. This may be due to the fact that total weight change and lattice parameter of phase $Zr_{0.33}U_{0.67}O_{2+x}$ depends on oxygen potential of the atmospheres, maximum temperature and time of heating which alters the oxygen content thereby changing the lattice parameter. In general, the lattice parameters of solid solution $(M_yU_{1-y})O_{2\pm x}$ (M = rare earths, lanthanides and actinides) are linearly related to metal ion and oxygen concentration [8].

Table 7
Thermal stability of ZrU_2O_7 in different atmospheres

Atmosphere	Temp. range (K)	Loss/Gain (% Wt.)	End product	Cubic cell parameter (Å)
Air	1173– 1323	+0.88	ZrO_2+α-$(U_3O_8)_{ss}$ [*a]	–
				–
CO_2	1213–1373	+0.41	–	–
	1373–1673	−1.82	$Zr_{0.33}U_{0.67}O_{2+x}$	5.310
He	1373–1673	−1.24	$Zr_{0.33}U_{0.67}O_{2+x}$	5.313
Ar/8%H_2	673–1173	−2.03	$Zr_{0.33}U_{0.67}O_{2+x}$	5.350

[a] α-$(U_3O_8)^*_{ss}$: a solid solution of ZrO_2 in α-(U_3O_8) phase.

Kinetic studies for the formation of ZrU_2O_7 and its oxidation were carried out in air using heating rate of 10 K min^{-1} up to 1473 K. The fraction of oxidized (α) phase with temperature due to oxidation of (A) $Zr_{0.33}U_{0.67}O_{2.00}$ and (B) ZrU_2O_7 in air are shown in Fig. 7. The fraction oxidized (α) is given by

$$\alpha = (W_t - W_0)/(W_f - W_0)$$

where W_t, W_0 and W_f are the masses at time t, initial mass and final mass, respectively. From, the Fig. 7, the sigmoidal reaction kinetics for oxidation of $Zr_{0.33}U_{0.67}O_{2.00}$ and ZrU_2O_7 can be visualized. The initial rate of oxidation is very low followed by gradually increasing oxidation rate up to a maximum and then tails off as the reaction approaches completion. The kinetic parameters were evaluated from the TG data, using non-isothermal heating process with the methods suggested by Zsako [28]. A computer program developed by Ravindran [29] was used for this analysis. The activation energies and pre-exponential factors obtained for the oxidation of $Zr_{0.33}U_{0.67}O_{2.00}$ and ZrU_2O_7 in air are given Table 8. The typical value of activation energy for oxidation of $Zr_{0.33}U_{0.67}O_{2.00}$ to ZrU_2O_7 is 94.1 kJ/mol. The oxidation process is governed by nucleation and growth mechanism as followed from the following relation:

$$g(\alpha) = -\ln(1-\alpha)$$

The observed activation energy for the formation of ZrU_2O_7 is close to that of U_3O_7 formation from un-irradiated UO_2 [21].

Table 8
Kinetics of preparation of ZrU_2O_7 and its oxidation in air

Starting compound	End product	α-Range	Mechanism	E_a (kJ/mol)	Z (s^{-1})
$Zr_{0.33}U_{0.67}O_{2.00}$	ZrU_2O_7	0.1–0.9	MAMP	94.1 ± 10	1.62×10^4
ZrU_2O_7	ZrO_2+U_3O_8	0.1–0.9	MAMP	524.2 ± 50	4.31×10^{19}

MAMP: $g(\alpha) = -\ln(1-\alpha)$.

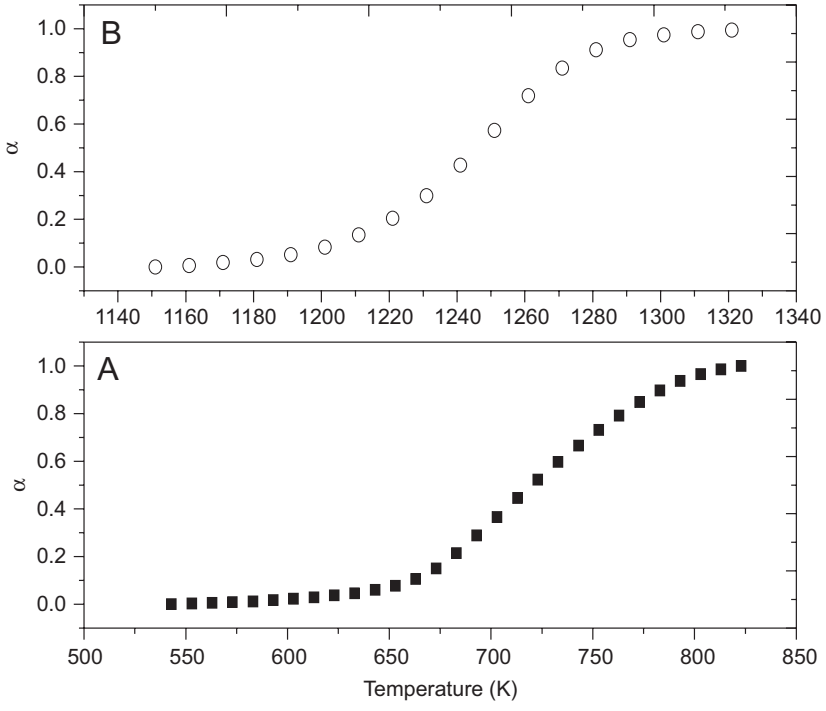

Fig. 7. α vs. temperature plot for: (A) $Zr_{0.33}U_{0.67}O_{2.00}$ and (B) ZrU_2O_7 in air.

However, the low temperature oxidation of UO_2 to U_3O_7 is diffusion controlled process because of adequate solubility of oxygen in UO_2 to form solid solution (UO_{2+x}). This leads to a concentration gradient inside the particle with steady decrease in O/U ratio from the surface to the interior. Similarly, oxidation of ZrU_2O_7 to Zr substituted U_3O_8 and excess ZrO_2 follows nucleation and growth mechanism following the relation $g(\alpha) = -\ln(1-\alpha)$. The typical activation energy for this process is 524.2 kJ/mol. However, the activation energy of formation of U_3O_8 from U_3O_7 following the same mechanism is reported in the range of 150–200 kJ/mol [21]. The higher activation energy obtained in the present studies may be due to higher temperature range (1173–1373 K) of oxidation of ZrU_2O_7, compared to U_3O_7 to U_3O_8 oxidation (673–873 K).

4. Conclusions

A new orthorhombically distorted fluorite type phase in Zr–U–O system is observed at the composition $Zr_{0.33}U_{0.67}O_{2.33}$ (ZrU_2O_7). The detailed chemical, theromogravimetric and crystal structure analyses indicate mixed valent U with interstitial oxygen in the fluorite lattice. The thermogravimetric studies in different atmospheres indicate a limited stability of this compound. In oxidizing atmosphere, it transforms to U_3O_8 type compound, while fluorite type solid solution is formed in the reducing atmosphere. Above 1173 K, the oxidation of ZrU_2O_7 leads to a mixture of Zr substituted U_3O_8 and ZrO_2. Higher activation energy (524 kJ/mol) is observed for the oxidation of this new phase compared to oxidation of U_3O_7 to U_3O_8. A nucleation and growth mechanism has been proposed for the oxidation behavior of ZrU_2O_7.

Acknowledgments

The authors are grateful to Dr. S. Kannan, Head, X-ray and Structural Studies Section of Fuel Chemistry Division and Dr. V. Venugopal, Director, Radiochemistry and Isotope Group for their constant encouragement during the course of this work. The authors thank Dr. S.K. Aggarwal, Head, Fuel Chemistry Division for critical reading of the manuscript. Also, we thank the anonymous reviewer to bring out the centric model for the structure solutions.

References

[1] R.E. Sykora, P.E. Raison, R.G. Haire, J. Solid State Chem. 178 (2005) 578.
[2] P. Li, I.W. Chen, J.E. Penner-Hahn, J. Am. Ceram. Soc. 77 (1994) 1281.
[3] P. Li, I.W. Chen, J.E. Penner-Hahn, J. Am. Ceram. Soc. 77 (1993) 118.
[4] V. Stolyarova, A. Shilov, M. Shultz, J. Nucl. Mater. 247 (1997) 41.
[5] H. Serizawa, K. Nakajima, Y. Arai, T. Yamashita, K. Kuramoto, H. Kinoshita, S. Yamanaka, M. Uno, K. Kurosaki, Prog. Nucl. Energy 38 (2001) 237.
[6] R.G. Haire, P.E. Raison, Z. Assefa, J. Nucl. Sci. Tech. (Suppl. 3) (2002) 616.
[7] P.E. Raison, R.G. Haire, Prog. Nucl. Energy 38 (3–4) (2001) 251.
[8] T. Fujino, C. Miyake, in: A.J. Freeman, C. Keller (Eds.), Handbook of Physics and Chemistry of Actinides, Elsevier, Amsterdam, 1991, p. 155.
[9] M. Yashima, T. Koura, Y. Du, M. Yoshimura, J. Am. Ceram. Soc. 79 (1996) 521.
[10] K. Une, M. Oguma, J. Am. Ceram. Soc. 66 (1983) C-179.
[11] I. Cohen, B.E. Schaner, J. Nucl. Mater. 9 (1963) 18.
[12] Y. Hinatsu, T. Fujino, J. Solid State Chem. 60 (1985) 244.
[13] R. Papiernik, B. Frit, Eur. J. Solid State Inorg. Chem. 25 (1988) 161.
[14] K.T. Pillai, R.V. Kamat, V.N. Vaidya, D.D. Sood, Mater. Chem. Phys. 44 (1996) 225.
[15] W. Davies, W. Gray, Talanta 11 (1964) 1203.
[16] A. Altomore, R. Caliandro, M. Camalli, C. Cuocci, C. Giacovazzo, A.G.G. Moliterni, R. Rizvi, J. Appl. Cryst. 37 (2004) 1025.
[17] J. Rodriguez-Carvajal, Multi-Pattern Rietveld Refinement Program FullProf, 2k Version 3.30, June 2005-LLB.
[18] A.C. Larson, R.B. van Dreele, GSAS: General Structure Analysis System, Los Alamos National Laboratory, Report LA-UR 86-748, 2000.
[19] S.K. Sali, N.K. Kulkarni, K. Krishnan, U.M. Kasar, S.K. Aggarwal, (to be published).
[20] J.G. Pepin, G.J. McCarthy, J. Am. Ceram. Soc. 64 (1981) 511.
[21] R.J. McEachern, P. Taylor, J. Nucl. Mater. 254 (1998) 87.
[22] R. Shirley, The Crysfire 2002 System for Automatic Powder Indexing.
[23] B.T.M. Willis, J. Chem. Soc. Faraday Trans. 283 (1989) 1073.
[24] G.C. Allen, N.R. Holmes, J. Nucl. Matter 223 (1995) 231.
[25] L. Nowicki, F. Garrido, A. Turos, L. Tome, J. Phys. Chem. Solids 61 (2000) 1789.
[26] D.J.M. Bevan, O. Greis, J. Strahle, Acta Cryst. A 36 (1980) 889.
[27] I.D. Brown, D. Altermatt, Acta Cryst. B 41 (1985) 244.
[28] J. Zsako, J. Phys. Chem. 72 (1968) 2406.
[29] P.V. Ravindran, Thermochim. Acta 39 (1980) 135.